

## Synthesis, Characterization, and Transport Properties of New Mixed Ionic–Electronic Conducting $\text{V}_2\text{O}_5$ –Polymer Electrolyte Xerogel Nanocomposites

Grant M. Kloster,<sup>†</sup> Joyce Albritton Thomas,<sup>‡,§</sup>  
Paul W. Brazis,<sup>§</sup> C. R. Kannewurf,<sup>§</sup> and  
Duward F. Shriver\*,<sup>†</sup>

Department of Chemistry, Northwestern University  
Evanston, Illinois 60208

Department of Electrical Engineering and  
Computer Science  
Northwestern University, Evanston, Illinois 60208

Received June 12, 1996

Revised Manuscript Received August 12, 1996

$\text{V}_2\text{O}_5$  xerogels can be synthesized by hydrolyzing vanadyl alkoxides or self-condensation of vanadic acid.<sup>1,2</sup> Sol–gel chemistry affords the possibility of making new  $\text{V}_2\text{O}_5$  composites with materials that cannot withstand the temperatures used in traditional synthesis of oxides (e.g., organic polymers). In this process mixing occurs at the molecular level, producing a nanocomposite. Nanocomposites are of special interest because they often exhibit properties that differ from those expected from the average of their individual components.<sup>3–5</sup> Sol–gel chemistry also may provide free-standing thin films or spin-coating substrates. Smyrl and co-workers prepared spin-coated  $\text{V}_2\text{O}_5$  xerogels as cathode materials that reversibly intercalate more than 3 equiv of lithium.<sup>6–8</sup> Kanatzidis and co-workers synthesized layered  $\text{V}_2\text{O}_5$  xerogel polymer composite bronzes with poly(pyrrole) and poly(thiophene) by the interaction of aqueous  $\text{V}_2\text{O}_5$  gels with the pyrrole or thiophene monomer.<sup>9,10</sup> They also prepared composites with poly(ethylene oxide) and studied the materials structure, electronic properties, and redox reactions with lithium iodide.<sup>11,12</sup> Ruiz-Hitzky and co-workers studied the structure and mixed protonic–electronic conductivity of the  $\text{V}_2\text{O}_5$ –crown ether composites they synthesized.<sup>13</sup>

The principle focus of the present research was to synthesize  $\text{V}_2\text{O}_5$ –polymer electrolyte mixed conducting xerogel nanocomposites and to characterize their charge transport properties. The polymer electrolyte (a-

$\text{PEO})_{20}\text{LiOTf}$  (a-PEO =  $(\text{CH}_2\text{O})_{0.1}(\text{CH}_2\text{CH}_2\text{O})_{0.9}$ , OTf =  $\text{CF}_3\text{SO}_3$ ) displays a room-temperature ionic conductivity of approximately  $10^{-5}$  S/cm, and it is an electronic insulator. The nanocomposites of  $\text{V}_2\text{O}_5$  and (a-PEO)<sub>n</sub>–LiOTf should exhibit mixed ionic–electronic conductivity with electronic conduction in the  $\text{V}_2\text{O}_5$  phase and ionic conduction in the polymer electrolyte. Vanadium oxide xerogels are also proton conductors. Previous research shows that hydrated vanadium oxide xerogels are proton conductors, but when the water content is reduced to  $\text{V}_2\text{O}_5 \cdot 0.5\text{H}_2\text{O}$  the protonic conductivity is negligible relative to the electronic conductivity ( $10^{-4}$ – $10^{-5}$  S/cm).<sup>2,14–16</sup> Intercalated compounds such as pyridine and crown ethers also dramatically reduce protonic conductivity in  $\text{V}_2\text{O}_5$  xerogels.<sup>13,16</sup>

Many unresolved issues still surround mixed conducting systems, although general features have been identified.<sup>17–22</sup> Several theoretical treatments predict enhanced ionic or electronic charge transport in mixed conductors when long-range Coulomb screening dominates,<sup>17,23–26</sup> but diminished electronic conductivity may result from ion gating or Coulomb trapping.<sup>27,28</sup>

The  $\text{V}_2\text{O}_5[(\text{a-PEO})_n\text{LiOTf}]$ , ( $n = 10$ – $24$ ,  $x = 0.01$ – $0.05$ ,  $[\text{V}]/[\text{EO}] = 4.0$ – $10.0$ ) composites were prepared by passing an aqueous solution of  $\text{NH}_4\text{VO}_3$  through a proton-exchange resin (Dowex 50-W, 50X-100) and then adding aqueous solutions of (a-PEO) and LiOTf in appropriate concentrations. Approximately 90% of the water was boiled away, and the resulting deep red material was poured into a Teflon dish. The remaining solvent was allowed to evaporate slowly, leaving a thin flexible dark red film about 100  $\mu\text{m}$  thick. X-ray diffraction reveals an increase in the interlayer spacing from 8.8  $\text{\AA}$  for the parent  $\text{V}_2\text{O}_5$  gel to 13.4  $\text{\AA}$  for the composite (Figure 1), which is comparable to the spacing for the  $\text{V}_2\text{O}_5$ –poly(ethylene oxide) composites.<sup>11</sup>

Infrared spectra of  $\text{V}_2\text{O}_5[(\text{a-PEO})_{10}\text{LiOTf}]_{0.05} \cdot n\text{H}_2\text{O}$  ( $[\text{V}]/[\text{EO}] = 10.0$ ) show bands at 519, 760, 914, and 1002  $\text{cm}^{-1}$  that are associated with the  $\text{V}_2\text{O}_5$  part of the composite. The band at 1002  $\text{cm}^{-1}$  is diagnostic of the  $\text{V}=\text{O}$  stretch.<sup>1,29,30</sup> Bands associated with (a-PEO)<sub>10</sub>–LiOTf are observed at 1048, 1108, 1174, 1233, 1256, and

\* Department of Chemistry.

† Department of Electrical Engineering and Computer Science.

‡ Present address: Ford Research Laboratory, Physics Department, Dearborn, MI 48121.

(1) Sanchez, C.; Nabavi, M.; Taulelle, F. *Mater. Res. Soc. Symp. Proc.* **1988**, *121*, 93–104.

(2) Livage, J. *Chem. Mater.* **1991**, *3*, 578–593.

(3) Dislich, H. *J. Non-Cryst. Solids* **1986**, *80*, 115–121.

(4) Mackenzie, J. D. *J. Non-Cryst. Solids* **1988**, *100*, 162–168.

(5) Komarneni, S. *J. Mater. Chem.* **1992**, *2*, 1219–1230.

(6) Passerini, S.; Chang, D.; Chu, X.; Le, D. B.; Smyrl, W. *Chem. Mater.* **1995**, *7*, 780–785.

(7) Le, D. B.; Passerini, S.; Tipton, A. L.; Owens, B. B.; Smyrl, W. H. *J. Electrochem. Soc.* **1995**, *142*, L102–L103.

(8) Park, H.-K.; Smyrl, W. H.; Ward, M. D. *J. Electrochem. Soc.* **1995**, *142*, 1068–1073.

(9) Kanatzidis, M. G.; Wu, C. G. *J. Am. Chem. Soc.* **1989**, *111*, 4139–4141.

(10) Kanatzidis, M. G.; Wu, C. G.; Marcy, H.; DeGroot, D. C.; Kannewurf, C. R. *Chem. Mater.* **1990**, *2*, 222–224.

(11) Liu, Y. J.; DeGroot, D. C.; Schindler, J. L.; Kannewurf, C. R.; Kanatzidis, M. G. *Chem. Mater.* **1991**, *3*, 992–994.

(12) Liu, Y. J.; Schindler, J. L.; DeGroot, D. C.; Kannewurf, C. R.; Hirpo, W.; Kanatzidis, M. G. *Chem. Mater.* **1996**, *8*, 525–534.

(13) Ruiz-Hitzky, E.; Aranda, P.; Casal, B. *J. Mater. Chem.* **1992**, *2*, 581–582.

(14) Barboux, P.; Baffier, N.; Morineau, R.; Livage, J. *Solid State Ionics* **1983**, *9/10*, 1073–1080.

(15) Livage, J.; Barboux, P.; Badot, J. C.; Baffier, N. *Mater. Res. Soc. Symp. Proc.* **1988**, *121*, 167–177.

(16) Casal, B.; Ruiz-Hitzky, E.; Crespin, M.; Tiné, D.; Galván, J. *C. J. Chem. Soc., Faraday Trans. 1* **1989**, *85*, 4167–4177.

(17) Huggins, R. A.; Huggins, J. M. *Macromolecules* **1977**, *10*, 889–892.

(18) Yokota, I.; Miyatani, S. *Solid State Ionics* **1981**, *3/4*, 17–21.

(19) Buck, R. P. *J. Electroanal. Chem.* **1987**, *219*, 23–48.

(20) Savéant, J. M. *J. Phys. Chem.* **1988**, *92*, 4526–4532.

(21) Ratner, M. A.; Shriver, D. F. *MRS Bull.* **1989**, *14*, 39–51.

(22) Yoo, H. I.; Lee, J.-H.; Martin, M.; Janek, J.; Schmarzried, A. *Solid State Ionics* **1994**, *67*, 317–322.

(23) Andrieux, C. P.; Savéant, J. M. *J. Phys. Chem.* **1988**, *92*, 6761–6767.

(24) Anson, I. C.; Blauch, D. N.; Savéant, J. M.; Shu, C. F. *J. Am. Chem. Soc.* **1991**, *113*, 1922.

(25) Blauch, D. N.; Savéant, J. M. *J. Am. Chem. Soc.* **1992**, *114*, 3323.

(26) Blauch, D. N.; Savéant, J. M. *J. Phys. Chem.* **1993**, *97*, G444.

(27) Lyon, L. A.; Ratner, M. A.; Hupp, J. T. *J. Electroanal. Chem.* **1995**, *387*, 109–113.

(28) Mott, N. *The Metal-Insulator Transition*; Taylor and Francis: London, 1974.

(29) Sanchez, C.; Livage, J.; Luzeau, G. *J. Raman Spectrosc.* **1982**, *12*, 68–72.

(30) Abello, L.; Husson, E.; Repelin, Y.; Luzeau, G. *J. Solid State Chem.* **1985**, *56*, 379–389.

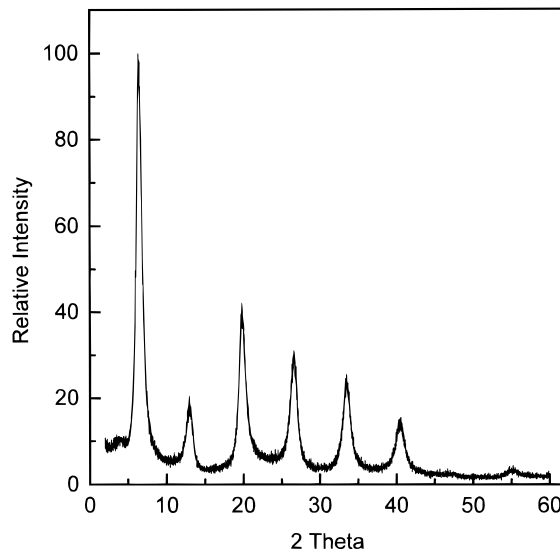


**Figure 1.** X-ray diffraction of a  $\text{V}_2\text{O}_5[(\text{a-PEO})_{10}\text{LiOTf}]_{0.05}$  thin film.

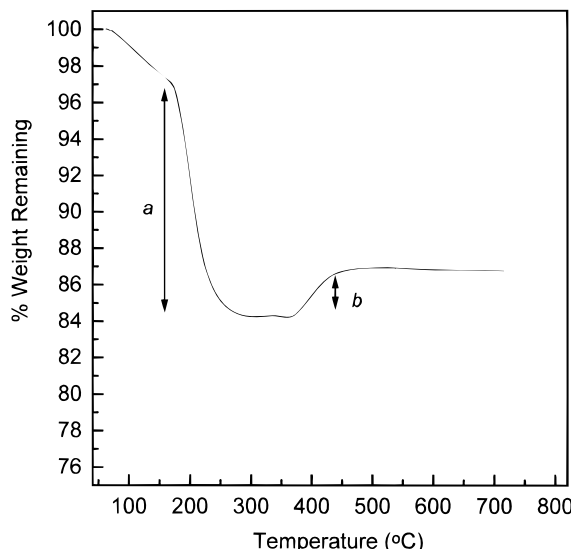


**Figure 2.** Thermogravimetric analysis of  $\text{V}_2\text{O}_5[(\text{a-PEO})_{20}\text{LiOTf}]_{0.01}$ . (a) Decomposition of  $(\text{a-PEO})_{10}\text{LiOTf}$  and loss of water. (b) Reaction with excess oxygen to form crystalline orthorhombic  $\text{V}_2\text{O}_5$ .

1348  $\text{cm}^{-1}$ , and water is observed at 1640 and 3400  $\text{cm}^{-1}$ . This infrared spectrum overlaps the spectra of the components. When the xerogels are heated at 120  $^{\circ}\text{C}$  in air for 24 h to remove weakly bound water, a band at 1734  $\text{cm}^{-1}$  appears, which indicates a ketonic oxygen and suggests partial oxidation of the polymer at this relatively low temperature.

It has been demonstrated that  $\text{V}_2\text{O}_5$  xerogels normally contain water in the ratio of 1.8  $\text{H}_2\text{O}$  molecules to 1  $\text{V}_2\text{O}_5$  unit and a small amount ( $\sim 1\%$ ) of reduced vanadium, presumably due to a reaction with the proton-exchange resin.<sup>2</sup> The water may be reversibly removed down to a ratio of  $\text{V}_2\text{O}_5 \cdot 0.5\text{H}_2\text{O}$  by heating the xerogel above 100  $^{\circ}\text{C}$  under  $\text{N}_2$  or in air. The remaining 0.5 mol of water is irreversibly removed by heating the  $\text{V}_2\text{O}_5$  xerogels above 200  $^{\circ}\text{C}$ , at which point crystalline  $\text{V}_2\text{O}_5$  is formed.<sup>2</sup>

The thermogram for  $\text{V}_2\text{O}_5[(\text{a-PEO})_{20}\text{LiOTf}]_{0.01}$  in air contains two main features (Figure 2). Between 180 and 280  $^{\circ}\text{C}$  part of the weight loss (a) corresponds to the evolution of water as indicated by the behavior of

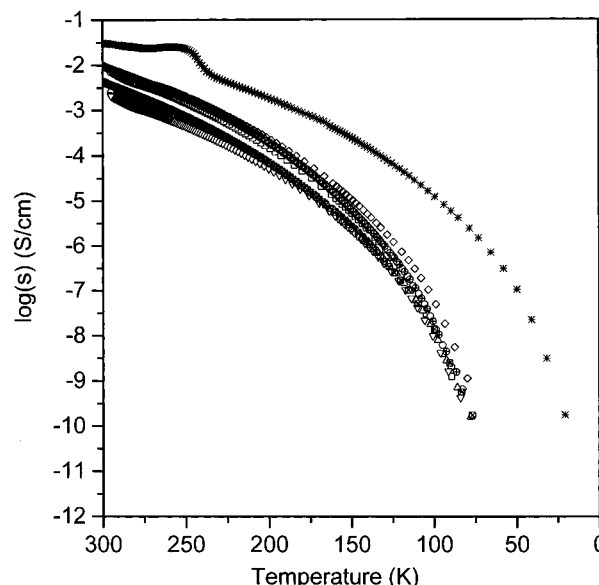


**Figure 3.** Variable-temperature electronic conductivity measured by the four point probe method. (\*) Polymer-free  $\text{V}_2\text{O}_5$  xerogel, (■)  $\text{V}_2\text{O}_5[(\text{a-PEO})_{0.5}\text{LiOTf}]_{0.05}$ , (□)  $\text{V}_2\text{O}_5[(\text{a-PEO})_{10}\text{LiOTf}]_{0.05}$ , (○)  $\text{V}_2\text{O}_5[(\text{a-PEO})_{11}\text{LiOTf}]_{0.045}$ , (△)  $\text{V}_2\text{O}_5[(\text{a-PEO})_{12}\text{LiOTf}]_{0.042}$ , (▽)  $\text{V}_2\text{O}_5[(\text{a-PEO})_{13}\text{LiOTf}]_{0.038}$ ,  $\otimes$   $\text{V}_2\text{O}_5[(\text{a-PEO})_{14}\text{LiOTf}]_{0.036}$ , and (◇)  $\text{V}_2\text{O}_5[(\text{a-PEO})_{19}\text{LiOTf}]_{0.026}$ .

polymer-free  $\text{V}_2\text{O}_5$  gels. Independent measurements on the pure polymer, the polymer electrolyte and the polymer-free  $\text{V}_2\text{O}_5$  xerogel indicate some polymer decomposition concomitant with the water loss in this temperature range. The high temperature, 180  $^{\circ}\text{C}$ , of the water evolution indicates that water is tightly bound in the composite. A small weight decrease before the water evolution at 180  $^{\circ}\text{C}$  suggests that some loosely bound intercalated water still exists in the composite. Between 375 and 425  $^{\circ}\text{C}$  the weight uptake (b) is interpreted as the reoxidation of  $\text{V}^{4+}$  produced at lower temperatures. This interpretation follows from the observation that feature (b) is absent when the process is performed in an inert atmosphere.

The electronic conductivity of the composites was measured parallel to the  $\text{V}_2\text{O}_5$  layers by the standard four-point probe method in a dry helium atmosphere, with gold electrodes attached across the top of each film. Polymer-free  $\text{V}_2\text{O}_5$  xerogels displayed room-temperature conductivities of  $3.6 \times 10^{-2}$  S/cm, and the temperature dependence indicates semiconductor behavior (Figure 3). A reproducible shoulder at 240 K is seen in the variable-temperature electronic conductivity data for the polymer-free  $\text{V}_2\text{O}_5$  xerogels in an inert atmosphere. This may be due to either a change in the interaction of the xerogel with the weakly bound water and/or a phase change. All of the  $\text{V}_2\text{O}_5[(\text{a-PEO})_n\text{LiOTf}]_x$  composites display lower conductivities than the polymer-free  $\text{V}_2\text{O}_5$  xerogel, and their conductivities decrease monotonically as temperature decreases. Room-temperature electronic conductivities range from  $1.1 \times 10^{-3}$  to  $4.6 \times 10^{-3}$  S/cm for composites with varying lithium triflate concentrations. No clear trend was evident for the variation in electronic conductivity with lithium triflate concentration.

The electronic conductivity data fit a variable-range hopping model, which has the general functional form  $\sigma = \sigma_0 \exp[-(T/T_0)^{-1/(z+1)}]$ , where  $z$  represents the dimensionality of the hopping mechanism ( $z = 1, 2, 3$ ).

The data fit one-, two-, or three-dimensional hopping mechanisms equally well. The accessible temperature range is presumably too narrow to distinguish between these models. As previously noted by Roth, it is difficult to determine the dimensionality of hopping mechanisms when conductivity data extend over a narrow temperature range.<sup>31</sup> A wider temperature range was not achievable because the material decomposes at high temperatures and exhibits very low conductivities at low temperatures.

The thermopower is negative for all composites, indicating that electrons are the majority charge carriers. This observation is consistent with thermopower measurements of previously studied  $V_2O_5$  xerogels and  $V_2O_5$  xerogel composites.<sup>11</sup> The magnitude of the thermopower is several hundred  $\mu V/K$ , which is typical for semiconductors. The thermopower data can be fit by a function characteristic of a variable-range hopping model,  $S = C_v T^{1/(z+1)} + C$ , where  $C_v$  is a variable-range hopping coefficient,  $C$  is an offset constant, and  $z$  is the dimensionality of the mechanism ( $z = 1, 2, 3$ ).<sup>32</sup> The data fit equally well to one-, two-, and three-dimensional models, as was observed for the electronic conductivity.

The transference numbers for electronic conductivity in the xerogels were measured parallel to the  $V_2O_5$  layers with gold electrodes by a two-probe method. The films were placed in a gastight cell where the relative humidity was controlled by varying the flow rates of dry and wet nitrogen through the cell. A 500 mV potential was placed across the films, and the current was monitored until it reached a steady state. The transference number was calculated as the ratio of the final current to the initial current. For  $V_2O_5[(a\text{-PEO})_{10}\text{-LiOTf}]_{0.05}$  in 0% relative humidity the electrons are the dominant charge carriers and the electronic transference number is 0.97. When the relative humidity is increased to 60% the electronic transference number decreases to 0.85, indicating that a smaller proportion of the charge is carried by the electrons.

Ac impedance measurements were performed on thin films of the nanocomposites placed between tantalum electrodes in a dry nitrogen atmosphere. Owing to the electrode geometry, the ac impedance measures total conductivity perpendicular to the film. By contrast the four-point probe method measures the electronic conductivity parallel to the film. A Nyquist plot of the ac impedance data at room temperature was fit by an

equivalent circuit containing a resistor in parallel with a capacitor and the dc conductivity was extracted. The total conductivity (electronic, ionic, and protonic) at room temperature perpendicular to the film of  $V_2O_5[(a\text{-PEO})_{20}\text{LiOTf}]_{0.01}$  is  $2.6 \times 10^{-8} \text{ S/cm}$ , 6 orders of magnitude less than the electronic conductivity parallel to the film, indicating that electronic charge-transport perpendicular to the film is virtually closed. However, the  $V_2O_5$ –polymer electrolyte composites do exhibit an order of magnitude greater total conductivity perpendicular to the film than the polymer and electrolyte-free  $V_2O_5$  xerogels. In contrast, the parallel electronic conductivity of the composites is less than the parallel electronic conductivity of the polymer and electrolyte-free  $V_2O_5$  xerogels. The greater total conductivity perpendicular to the films in the composite material indicates that the ionic conductivity of the  $(a\text{-PEO})_n\text{LiOTf}$  plays a role in the perpendicular conductivity. Presumably the  $(a\text{-PEO})_n\text{LiOTf}$  forms ionic conduction pathways between the edges of the  $V_2O_5$  layers, as seen for polymer electrolytes intercalated in clays where electronic conductivity is not an issue.<sup>33,34</sup>

In summary, the new  $V_2O_5[(a\text{-PEO})_n\text{LiOTf}]_x$  xerogel nanocomposites are mixed ionic–electronic conductors. The polymer electrolyte displaces much of the weakly bound water, but tightly bound water remains. The nanocomposites exhibit high electronic conductivity parallel to the films while conduction pathways perpendicular to the films appear to be virtually closed. The mechanism of in-plane electronic conduction best fits a variable-range hopping model, but the dimensionality of the model is difficult to determine. Variation of the lithium triflate concentration alters the electronic conductivity in a minor and currently unpredictable manner. Around 120 °C infrared spectra demonstrate partial oxidation of intercalated PEO by the  $V_2O_5$ .

**Acknowledgment.** This work was supported by the MRL Program of the National Science Foundation through the Materials Research Center (DMR 91-120521), the Department of Basic Energy Science (DEFG02-85ER45220-08), and the Department of Education. We thank Dr. Rabin Bisssesur for his helpful suggestions on the chemistry of intercalated systems and Professor Mark Ratner for sharing his insight on mixed conducting systems.

CM9603361

(31) Roth, S., Roth, S., Eds.; Elsevier Publishers B.V.: North-Holland, 1991; p 377.

(32) Mott, N. *Conduction in Non-Crystalline Materials*; Oxford University Press: New York, 1987.

(33) Aranda, P.; Galvan, J.; Casal, B.; Ruiz-Hitzky, E. *Electrochim. Acta* **1992**, *37*, 1573.

(34) Hutchison, C.; Bisssesur, R.; Shriver, D. *Chem. Mater.*, in press.